Available online at www.sciencedirect.com
ScienceDirect
Thin Solid Films 516 (2008) 7627–7635
www.elsevier.com/locate/tsf

Adhesion strength measurement of polymer dielectric interfaces using laser spallation technique

Soma Sekhar V. Kandula [a], Cheryl D. Hartfield [b,1], Philippe H. Geubelle [a], Nancy R. Sottos [c,*]

[a] Department of Aerospace Engineering, University of Illinois at Urbana-Champaign, Urbana, IL 61801, USA
[b] Semiconductor Packaging and Development, Texas Instruments, Dallas, TX 75243, USA
[c] Department of Materials Science and Engineering, University of Illinois at Urbana-Champaign, Urbana, IL 61801, USA

Received 26 November 2007; received in revised form 8 May 2008; accepted 15 May 2008
Available online 29 May 2008

Abstract

A laser-induced spallation technique is employed to obtain the critical interface strength of the poly-*p*-phenylenebenzobisoxazole (PBO) polymer and silicon nitride (Si_xN_y) interface in a silicon (Si)/Si_xN_y/PBO multilayered wafer. Stress wave propagation in this multilayered material is analyzed both analytically and numerically. The influence of processing conditions, substrate surface morphology and PBO formulations on the interface adhesion strength is investigated. The interface strength values correlate strongly with the PBO formulation and surface roughness of the substrate. Effect of autoclaving on the interface adhesion strength is also investigated.

Keywords: Adhesion; Laser spallation; Delamination; Interface failure; Wave propagation

1. Introduction

Thin dielectric polymer films made of poly-*p*-phenylenebenzobisoxazole (PBO) are used as stress buffers in various flip chip integrated circuit packages to reduce the stress between silicon passivation layers and mold compound. Due to the disparity of material properties between the polymer PBO and interlayer passivation materials, PBO/passivation interface failure is a reliability concern. Hence, characterizing the influence of different PBO formulations, processing conditions and quality of the substrate on the interface strength is critical for designing a robust and reliable interface.

An overview of several thin film adhesion test methods including peel, stud-pull, scratch, bulge, four-point bending and superlayer is given in a recent publication by Lacombe [1]. The three most common methods that are routinely applied in the microelectronic industry to estimate the thin film interfacial adhesion are peel, stud-pull and four-point bending tests. In general, peel tests subject the thin film to high tensile stresses. If the films have a low tensile strength, which is the case with PBO, there is a possibility of film failure prior to interfacial delamination. To avoid tensile film failure in a peel test, Shih et al. [2] processed an additional backing layer onto the top of a polymeric thin film deposited on ceramic substrate. In a stud-pull test, a rigid metallic stud is bonded to the polymeric film with epoxy. The stud is then pulled at a controlled rate until a critical force is reached when interfacial failure occurs. In a preliminary study, stud-pull tests were performed to characterize the PBO/silicon nitride (Si_xN_y) interfacial adhesion. The adhesion levels were so high, the films had to be scored to enable pull-off. Even after scoring, only a qualitative comparison of adhesion differences between film formulations was possible.

For some thin film/substrate combinations, the interfacial fracture toughness can be extracted from four-point bend [3,4], blister [5] or superlayer [6–8] tests. The preparation of four-point bend specimens involves bonding two geometrically identical thin film samples together with epoxy. The effectiveness and repeatability of the test relies on generation and propagation of a pre-crack along the interface of interest. Proper specimen preparation is often time consuming due to the difficulties in introducing the pre-

* Corresponding author.
E-mail address: n-sottos@uiuc.edu (N.R. Sottos).
[1] Present address of CDH: Omniprobe Inc., Dallas, TX 75238.

0040-6090/$ - see front matter © 2008 Elsevier B.V. All rights reserved.
doi:10.1016/j.tsf.2008.05.033

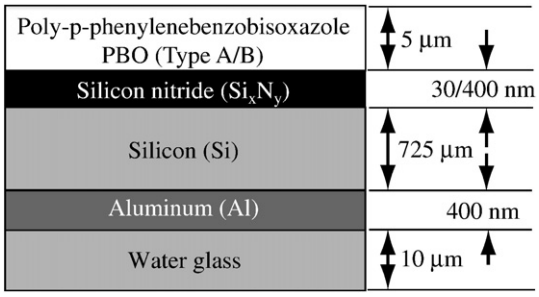

Fig. 1. Schematic of the Si/Si_xN_y/PBO multilayered sample used in the spallation study.

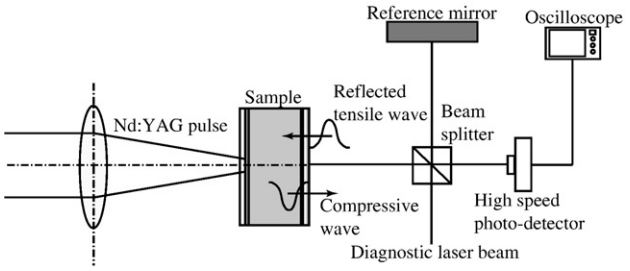

Fig. 2. Schematic of the laser spallation experimental setup.

crack. Blister and superlayer techniques also require significant sample preparation and are not practical for rapid PBO interface characterization.

In contrast to the quasi-static loading in most adhesion tests, the laser spallation technique [9–22] employs high amplitude laser-induced acoustic stress pulses to dynamically load a thin film interface. These pulses have sharp temporal rise and fall times and subject the thin film to strain rates of the order 10^7/s. At these high strain rates, the effect of inelastic deformations is reduced.

Vossen [23] adapted the spallation technique to estimate the bond strength of millimeter thick aluminum (Al) films on substrates using a high energy laser-induced acoustic pulse loading. For substrates that were transparent to the wavelength of the light emitted by the laser, an absorbing layer was coated on the back side of the substrate prior to the loading process. A laser pulse impinging the absorbing layer generated a compressive acoustic pulse, that loaded the interface after reflection from the free surface in a non-contact manner.

Gupta et al. [12–15] and Yuan et al. [16–19] extended Vossen's technique to investigate a wide variety of thin film interfaces. More recently, Gupta et al. [12] and Jain et al. [24] applied the laser spallation technique to polyimide films on Si/Si_xN_y wafers to understand the effects of humidity and temperature on the tensile strength of the interface. After determination of the critical laser power at which the spallation initiated, the interface strength was extracted through a combination of experimental calibration and corresponding one-dimensional wave propagation simulations.

In this work, we apply the laser spallation technique to measure the adhesive strength of the PBO/Si_xN_y interface in a multilayer thin film stack. Through careful analysis of the stress wave propagation through multiple layers, a simple analytical relationship is obtained to calculate the interface stress from the displacement measurements. The laser spallation test protocol is able to quantify changes in adhesion due to PBO composition, Si_xN_y roughness and different processing conditions.

2. Experimental technique

2.1. Sample preparation

The configuration of the PBO thin film/substrate multilayered specimen is depicted in Fig. 1. Four different specimen combinations, listed in Table 1, were fabricated using two different PBO formulations, PBO Type A and PBO Type B, and two different Si_xN_y dielectric interlayer thicknesses, 30 nm and 400 nm. Single side polished single crystal Si substrates, with a (100) orientation had an average thickness of 725 μm. A low pressure chemical vapor deposition process was used to grow the interlayer Si_xN_y dielectric on the polished side of silicon substrates. Surface roughness of the interlayers was characterized by atomic force microscope scans of a 10 μm by 10 μm area on the Si_xN_y surface. The root mean square roughness parameter for the 30 nm and 400 nm Si_xN_y thickness layers was 8.2 Å and 32 Å, respectively. Samples were subjected to a dehydration bake to remove excess solvents left on the wafer. The influence of this processing step on the interfacial adhesion strength was examined by fabricating and testing an additional group of PBO Type B films on a 30 nm Si_xN_y

Table 1
Details of the spallation specimens and measured interface strength values

PBO formulation type	Si_xN_y thickness (nm)	Interface strength (GPa)
A	30	0.24
A	400	0.28
B	30	0.28
B*	30	0.24
B	400	0.34

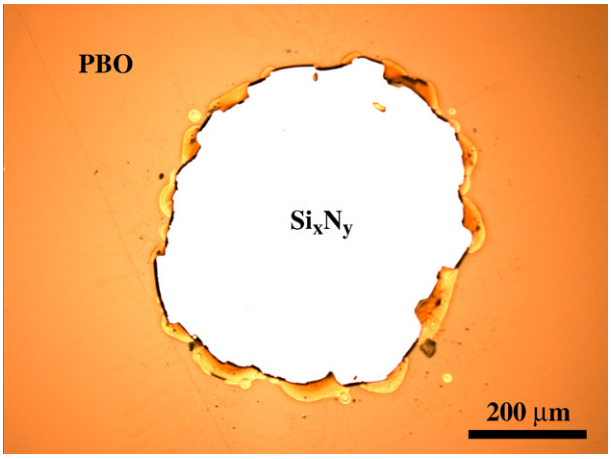

Fig. 3. Optical micrograph of a spalled sample showing a complete interfacial delamination of PBO.

interlayer without a dehydration bake. This group of samples hereafter is denoted by PBO Type B*.

For all samples, the back surface of the Si substrate (Fig. 1) was coated with a 400 nm thick Al absorbing layer using a Temescal electron beam evaporator, equipped with planetary substrate holders which were rotated during the deposition to maintain uniformity of the Al thickness. A constraining water glass layer was spun on the top of the Al absorbing layer with a nominal thickness of 10 μm.

2.2. Laser spallation setup

The laser spallation setup is shown schematically in Fig. 2 along with the interferometric diagnostics used to track the out-of-plane displacement history of the sample free surface. A 1064 nm light pulse generated by a Q-switched Nd:YAG laser with a rise time of about 5 ns is focused to a circular spot of 1.6 mm in diameter (from a nominal beam diameter of 3.5 mm) on the back side of the substrate using conventional optics. The laser-induced ablation of the confined Al absorbing layer results in the generation of a high amplitude compressive acoustic pulse, with a rise time comparable to that of the impinging light pulse. Upon reaching the free surface of the test film, the compressive pulse reflects back as a tensile pulse and loads the interface of interest in tension. If the magnitude of this tensile stress pulse is greater than the interfacial adhesion strength, the test film spalls from the substrate. A typical failure pattern of a spalled PBO film is shown in Fig. 3.

Varying the laser fluence from 0 to 65 mJ/mm^2 results in compressive stress pulse amplitudes varying between 0 to 3.5 GPa depending on the spot size and confining layer thickness. Decreasing the spot size of the YAG beam and increasing the water glass confinement results in an increase of the amplitude of the compressive stress pulse and vice versa. Interface strength is determined by increasing the laser fluence until a compressive pulse is generated with an amplitude sufficient to fail the interface of interest.

Out-of-plane displacements are measured as a function of time with a Michelson interferometer. Fringe data due to the motion of the free surface of the sample are acquired using a high band width digital oscilloscope (LeCroy LC584A, 1 GHz with a sampling rate of 8 GHz in single shot mode) in combination with a high speed photodetector (EOT 2000 N). The free surface displacement history $u(t)$ is calculated from the Doppler shift following the procedure adopted by Barker [25,26] through

$$u(t) = \frac{\lambda_0 n(t)}{2}, \tag{1}$$

where λ_0 (514.5 nm) is the wavelength of the Argon laser light used for probing the sample motion. The fringe count $n(t)$, as a

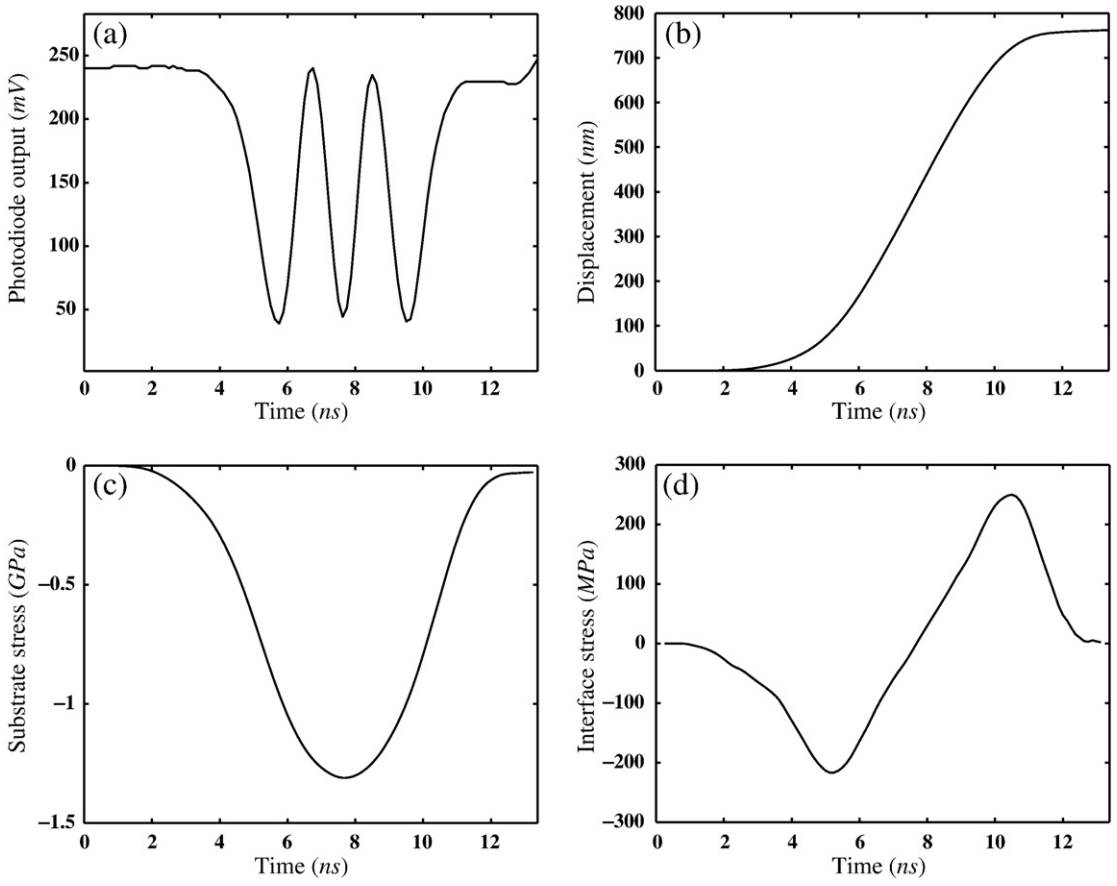

Fig. 4. Representative data obtained during laser spallation testing of a 1.7 μm thick Al film deposited on a Si substrate: (a) photodiode output as captured by the oscilloscope, (b) displacement of the sample free surface, (c) substrate stress and (d) interface stress.

function of time t, is determined from the intensity pattern recorded by the oscilloscope using

$$I(t) = \frac{I_{max} + I_{min}}{2} + \frac{I_{max} - I_{min}}{2}\sin(2\pi n(t) + \phi), \quad (2)$$

where I_{max} and I_{min} represent the maximum and minimum intensities of the interference fringes, respectively, and ϕ denotes the phase angle. For a simple bi-material interface, the evolution of the substrate stress pulse (σ_{sub}) and the interface stress (σ_{int}) are readily determined from the displacement history using the principles of one-dimensional wave mechanics [9]. When the thickness of the test film (h) is smaller than the spatial spread of substrate pulse during the rise time (t_{rise}), i.e., $h << (C_d)_{film} * t_{rise}$, the following thin film equations are valid for calculation of the substrate and interface stresses

$$\sigma_{sub}(t) = -\frac{1}{2}(\varrho C_d)_{sub}\frac{du}{dt}, \quad (3)$$

$$\sigma_{int}(t) = -(\varrho h)_{film}\frac{d^2u}{dt^2}, \quad (4)$$

where ϱ is the density and C_d is the dilatational wave speed, the subscripts *sub* and *film* represent substrate and thin film, respectively. When the film thickness h is comparable to $(C_d)_{film} * t_{rise}$, the following thick film equations more accurately represent the stress history:

$$\sigma_{sub}(t) = -\frac{(\varrho C_d)_{sub}}{4}\frac{d}{dt}\left[u\left(t - \frac{h}{(C_d)_{film}}\right) + u\left(t + \frac{h}{(C_d)_{film}}\right)\right] + \frac{(\varrho C_d)_{film}}{4}\frac{d}{dt}\left[u\left(t - \frac{h}{(C_d)_{film}}\right) - u\left(t + \frac{h}{(C_d)_{film}}\right)\right] \quad (5)$$

$$\sigma_{int}(t) = \frac{(\varrho C_d)_{film}}{2}\frac{d}{dt}\left[u\left(t - \frac{h}{(C_d)_{film}}\right) - u\left(t + \frac{h}{(C_d)_{film}}\right)\right]. \quad (6)$$

A representative interference fringe pattern obtained during the spallation of a 1.7 μm thick Al film on 725 μm thick Si substrate accompanied by the corresponding surface displacement, substrate stress and interface stress histories is shown in Fig. 4. Since the Al film is relatively thin, Eqs. (3) and (4) are used to calculate the stress history. For the PBO films under investigation, the wave propagation analysis is more complicated due to the presence of the Si_xN_y interlayer. A detailed analysis of wave propagation in the current specimen configuration is provided in the next section.

3. Analysis of one-dimensional wave propagation in multilayered media

The evolution of stresses at the Si_xN_y and PBO interface are predicted through analysis of one-dimensional wave propagation in the three layer Si/ Si_xN_y/PBO stack. Details of the analysis are described in the Appendix. We consider the simple case of a finite layer of Si_xN_y sandwiched between two semi-infinite media made of Si and PBO (Fig. A.1). This specific geometry is chosen to understand the effect of the thickness of the Si_xN_y layer on the stress wave transfer in the three layer stack. The shape of compressive substrate stress pulse is of unit magnitude and temporally resembles the pulse generated by the YAG laser in the experimental study, which is Gaussian shaped with a rise time of 5 ns. The material properties for the simulation are summarized in Table 2. In this analysis, we chose four different thicknesses of Si_xN_y interlayer, h=25 nm, 250 nm, 2.5 μm and 25 μm, to represent a wide range of possible Si_xN_y dielectric interlayer thicknesses.

The development of stress at the interface between Si_xN_y and PBO for the various thicknesses is summarized in Fig. 5. The magnitude of the interface stresses decreases with increasing h and is more pronounced at higher thicknesses (h=2.5 μm). The effect is negligible for lower values of h where the response converges to a single curve. We also determined the number of reflections (Fig. A.1) the pulse encounters while propagating across the interlayer as 1762, 176, 17 and 1 for h values 25 nm, 250 nm, 2.5 μm and 25 μm, respectively. Every reflection at the interface contributes to the development of stress at the interface of interest. For the current specimen configuration, all the additional terms are compressive in nature and may interfere depending on the thickness and dilatational wave speed in the interlayer. For the case where h=25 μm, these reflections are compressive but spread out without interfering, resulting in a lower interface stress value. In contrast, the interface stress increases in amplitude with increasing number of interfering reflections as demonstrated by the curves corresponding with lower h values. The limiting upper bound on the magnitude is achieved for infinite number of reflections which corresponds to the case where the Si_xN_y layer thickness collapses to a zero value. The Si_xN_y interlayer then reaches a homogenized stress state, i.e., the stress across the interlayer is constant at any instant in time and does not influence the magnitude of the interface stress. From this analysis, we conclude that the Si_xN_y interlayers considered in this study (h=30 nm, 400 nm) do not significantly alter the stress wave propagation and therefore need not be considered in predicting the stress evolving at the interface.

We also analyzed pulses of varied temporal shapes using normalized Beta functions characterized by the parameters β

Table 2
Thin film material properties for multilayer spallation specimens

Material	Young's modulus (E) (GPa)	Density (Q) (kg/m^3)	Poisson's ratio (ν)
Si (100)	130	2330	0.28
Si_xN_y	220	3400	0.25
PBO	3.1	1400	0.3
Al	70	2710	0.35

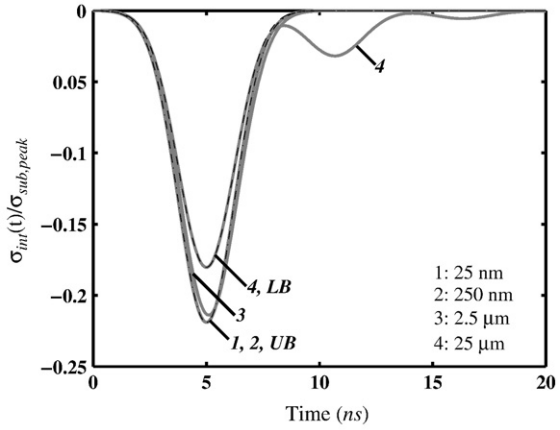

Fig. 5. Evolution of interface stress, under the action of a unit magnitude Gaussian shaped substrate stress pulse, at the Si_xN_y/PBO interface for various thickness values of the Si_xN_y layer: (1) 25 nm, (2) 250 nm, (3) 2.5 μm and (4) 25 μm. The black dashed curves denoted by UB and LB respectively represent the upper and lower bounds on the interface stress values.

and γ to emulate a wide spectrum of rise times of the substrate pulse as described by:

$$\sigma_{\text{sub}}(X) = \frac{X^{\beta-1}(1-X)^{\gamma-1}}{X_m^{\beta-1}(1-X_m)^{\gamma-1}}; X(t) = \frac{t}{t_{\text{pulse}}};$$
$$X_m = \frac{\beta-1}{\beta+\gamma-2} \text{ for } \beta+\gamma \neq 2 \quad (7)$$

For comparison purposes, we maintained the total time of the pulse (t_{pulse}) as the Nd:YAG generated laser pulse duration in our experiment. The evolution of the Si/PBO interface stress for various substrate pulses with different rise times, dictated by the parameters β and γ is shown in Fig. 6. As discussed above, we neglected the Si_xN_y layer and used the bilayer equation developed for thick films (Eq. (6)). The evolution of the interface stress depends on the shape of the substrate pulse. However, the peak of the interface stress pulse is invariant for the range of the rise times of the pulses considered. Examination of the reflection and transmission coefficients each time the pulse encounters at the interface during its travel reveals that the second term in Eq. (A.3) dominates the interface stress pulse history. For the current combination of specimen geometry and YAG pulse profile, the relation between the peak of the interface stress to the peak of the substrate stress is approximated by the simple relation

$$\sigma_{\text{int,peak}} = -\frac{4\alpha}{(1+\alpha)^2}\sigma_{\text{sub,peak}}, \quad (8)$$

where α is the impedance mismatch ratio. For the current Si/PBO bi-material system, the peak magnitudes of the substrate and interfaces stresses are related by

$$\sigma_{\text{int,peak}} = -0.39\sigma_{\text{sub,peak}}, \quad (9)$$

which predicts a maximum tensile interface stress as 0.39 GPa when loaded by a compressive substrate stress of unit magnitude (excellent agreement with exact calculations in Fig. 6). To verify our simplified analytical model, we simulated the one-dimensional wave propagation numerically with finite elements using the specimen geometry in Fig. 1 with an interlayer Si_xN_y thickness of 400 nm and a substrate pulse defined by the Beta function with parameters β=4 and γ=2. The finite element prediction of the stress evolution at the interface between Si_xN_y and PBO is plotted in Fig. 6 using a dotted curve. Excellent agreement is achieved between the numerical and analytical solutions.

4. Experimental protocol

Our experimental protocol to measure the interface strength consisted of three steps. First, a series of Si/Si_xN_y calibration samples were prepared with no PBO layer. These samples were then tested over a range of laser fluences to calibrate the peak of the substrate stress as a function of laser power. The third step was the testing of Si/Si_xN_y/PBO samples to determine the critical laser fluence for interfacial failure. The interface strength was extracted from the critical laser fluence using the calibration data along with Eq. (8).

4.1. Calibration procedure

The calibration sample was nearly identical to test specimens described in Fig. 1 and consisted of a 30 nm thick Si_xN_y layer deposited on 750 μm thick Si wafer with no PBO layer. In addition, a 100 nm thick Al reflective layer was deposited by e-beam evaporation to improve the signal for interferometric measurements.

The calibration samples were tested at laser fluences ranging from 22.5 to 67.5 mJ/mm^2 in increments of 1.88 mJ/mm^2. Eight tests were performed at each laser fluence. Interferometric data was acquired for each test and the corresponding substrate stress pulse was calculated as described in Section 2. The maximum value of the substrate pulses were averaged at each laser

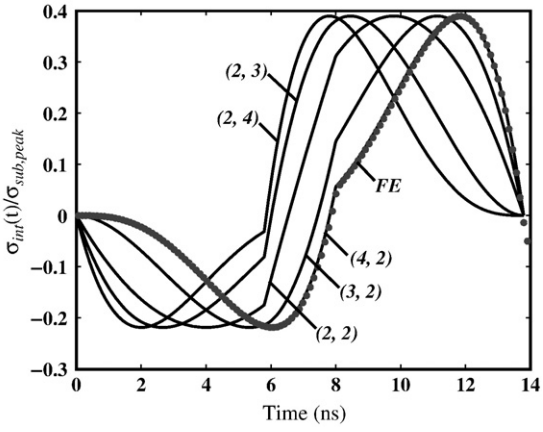

Fig. 6. Evolution of interface stress, normalized by the peak of the substrate stress pulse, at the Si/PBO interface for various parameters of the beta functions, (β, γ), shown in parentheses. The dotted curve corresponds to the finite element (FE) simulation obtained for β=4, γ=2.

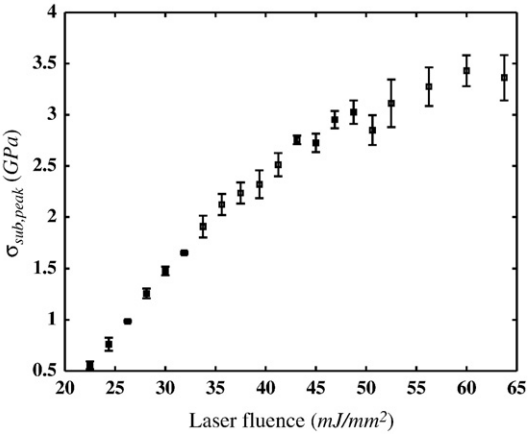

Fig. 7. Peak of the substrate stress pulse calibrated using a Si/Si_xN_y (30 nm)/Al sample as a function of laser fluence. Error bars represent one standard deviation from the mean value.

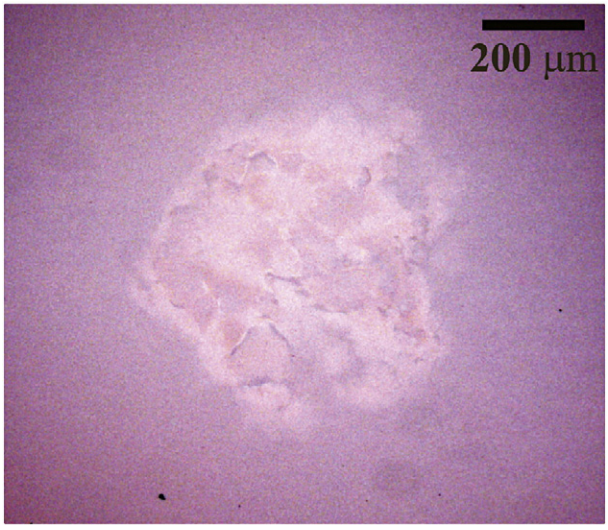

Fig. 8. Optical micrograph showing subsurface delamination in a Si/Si_xN_y/PBO sample.

fluence. As shown in Fig. 7, the amplitude of the substrate pulse increased with the applied laser power before saturating at a magnitude of 3.5 GPa at full laser power. Silicon cleavage has been observed previously in laser spallation testing [10] and is undesirable prior to interfacial failure. In the current experiments, the PBO/Si_xN_y interface failed well below Si cleavage occurred.

4.2. Determination of critical laser fluence

For each of the PBO samples listed in Table 1, the critical laser fluence for failure was determined by first testing the samples at high fluence levels where failure was confirmed optically, followed by successively decreasing the fluence level in decrements of 0.38 mJ/mm^2 until failure was no longer observed. The critical fluence level, which corresponds to the onset of failure initiation, was determined by optical examination of the spalled sample under fluorescent light. Interfacial failure initiated at low fluences at the Si_xN_y/PBO interface, 5 μm below the free surface, prior to complete spallation. An optical micrograph showing one such subsurface interfacial delamination is shown in Fig. 8. After obtaining the critical laser fluence, the interface strengths were calculated using the magnitude of the critical substrate stress obtained from the calibration curve and Eq. (8).

4.3. Validation of the calibration procedure

The calibration protocol described above was validated through direct interferometric measurements. The critical laser fluence for a PBO Type B film with Si_xN_y thickness of 400 nm was determined first using the procedure outlined in the previous section. For interferometric measurements, a 75 nm thick aluminum film was deposited on the PBO film to make the surface reflective. The PBO specimens were then tested at a fluence level (22 mJ/mm^2) less than the critical value for interfacial failure. Displacements at the free surface were obtained using the displacement interferometer setup and plotted in Fig. 9. The displacement profile was then predicted numerically using the substrate pulse profile measured in the calibration experiments at the same laser fluence. The numerical method is a combination of an explicit central difference time stepping scheme and one-dimensional two-node finite element scheme to capture the transient and spatial response, respectively. The predicted evolution of the displacements is also plotted in Fig. 9 for comparison. The excellent agreement between these results validates the experimental protocol for determining interfacial strength in the Si/ Si_xN_y/PBO sample without direct interferometric measurement, as well as the choice of the material parameters used in the analysis.

5. Results and discussion

5.1. Qualitative failure characterization

By performing spallation experiments at high laser fluences, where delamination and in some cases complete

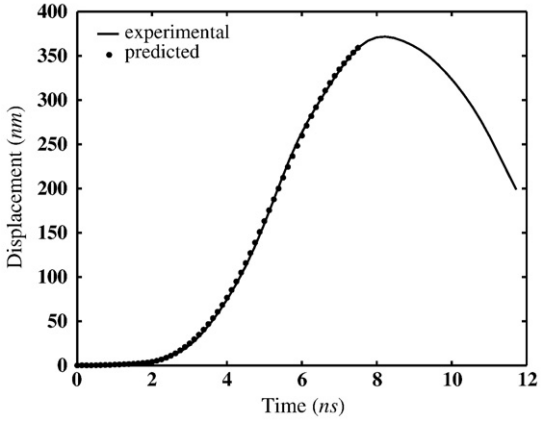

Fig. 9. Comparison of predicted and measured displacement of the PBO free surface, as a function of time, under the influence of a substrate pulse generated at a laser fluence less than critical fluence for failure initiation.

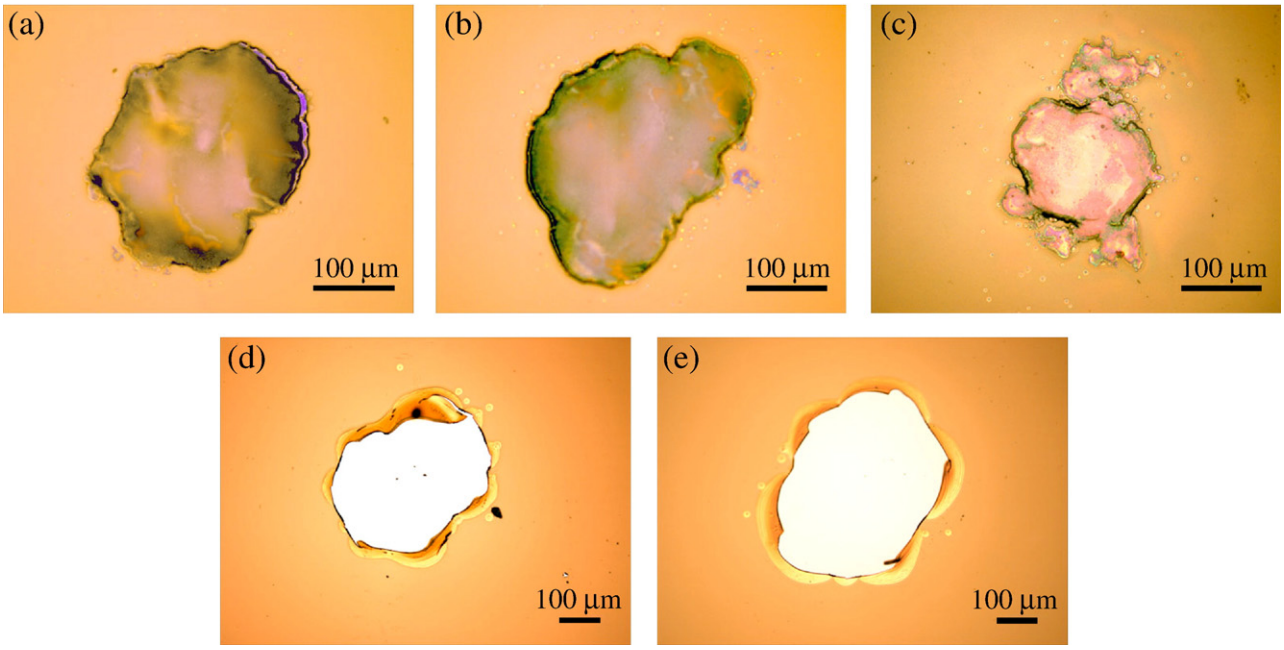

Fig. 10. Optical images of spallation damage in all the PBO samples impinged at high Nd:YAG laser fluence (50 mJ/mm^2) above the critical fluence for initiation of interface failure. (a) 30 nm Si_xN_y/Type B PBO, (b) 30 nm Si_xN_y/Type B* PBO, (c) 400 nm Si_xN_y/Type B PBO, (d) 30 nm Si_xN_y/Type A PBO, (e) 400 nm Si_xN_y/Type A PBO.

spallation were visible, we qualitatively assessed the PBO film adhesion based on the observed failure patterns. Fig. 10 contains optical images of different PBO film failures at a high fluence (50 mJ/mm^2), larger than the critical fluence for initiating interface failure. For the same laser fluence, the PBO films with Type A formulation completely delaminated from the substrate while the PBO films with Type B formulation only show the onset of delamination. These delamination patterns qualitatively indicate that PBO adhesion is better for Type B formulation than that of Type A.

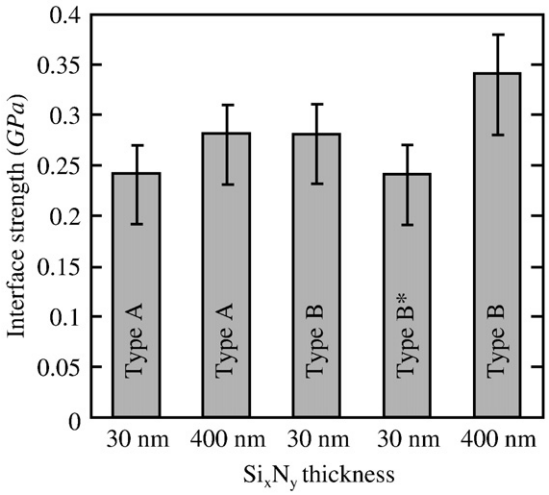

Fig. 11. Comparison of the PBO/Si_xN_y interface strengths of various Si/Si_xN_y/PBO specimens measured using laser spallation technique. The error bars were calculated by estimating the uncertainty in the value of Young's modulus of the PBO film (±1 GPa) and the variation in the peak magnitude of the stress pulse at the critical laser fluence. * denotes the no dehydration bake sample.

5.2. Interface strength

The interface strength was determined for all the samples types listed in Table 1 using the experimental protocol described in Section 4. The bar plot in Fig. 11 compares the final interface strengths. The measured interface strengths of PBO Type B formulation are 21% and 16% greater than that of PBO Type A for the Si_xN_y thicknesses of 400 nm and 30 nm, respectively. Interestingly, the samples with Si_xN_y thickness of 400 nm had higher interface strengths than other samples made of the same PBO type with a 30 nm thick interlayer. Although the thickness of the Si_xN_y interlayer does not influence the wave propagation, surface roughness may play a major role in the PBO film adhesion, as the surface of the 400 nm thick interlayer was significantly rougher than the 30 nm thick layer. The increase of interface strength with increasing surface roughness is consistent with the interface toughness measurements reported by Ren et al. [27] for thin nickel films on titanium substrates. Also, the sample with no dehydration bake during thin film processing showed a 40 MPa loss in adhesion strength when compared with the dehydration baked sample with the same Si_xN_y layer thickness. The error bars were calculated by estimating the uncertainty in the value of Young's modulus of the PBO film (± 1 GPa) and the variation in the peak magnitude of the stress pulse at the critical laser fluence.

In addition, we examined the effects of autoclaving on the interface strength of PBO Type B formulated specimens. The

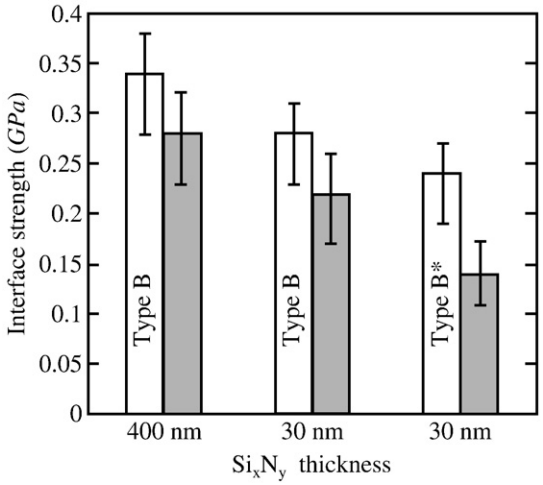

Fig. 12. Comparison of the interface strengths of Type B PBO samples before (left, white) and after autoclaving (right, grey). The error bars have the same significance as in Fig. 11.

test samples were autoclaved at one atmospheric pressure at 121 °C for 48 h. The interface strengths were determined for the autoclaved samples following the same experimental protocol. Fig. 12 compares the interface strengths of all the three PBO Type B samples before and after the autoclave process. The interface strength of samples with dehydration bake degraded by 18% and 21% for 30 nm and 400 nm Si_xN_y , respectively. Samples with out a dehydration bake exhibited a 42% decrease in the interface strength.

In summary, the Si/Si_xN_y/PBO samples made of Type B PBO polymer formulation on a 400 nm Si_xN_y with dehydration bake have the highest interface strength. The thin film interface strength is enhanced by the increased surface roughness of the substrate and the dehydration bake process. The interface strengths of all the Si/Si_xN_y/PBO type specimens were calculated based on a single set of calibration data. This strategy combined with the simplified analysis leads to time savings and greatly improved sensitivity in comparison with the four-point bend and stud-pull techniques typically employed in the microelectronics industry to measure adhesion of PBO films to the substrates.

6. Conclusions

Using the laser spallation technique, we were able to quantify interface strengths of PBO films deposited on Si_xN_y passivated single crystal Si substrates. For the Nd:YAG laser pulses used in this study, the thin Si_xN_y layers did not influence wave propagation and were neglected in the analysis. Furthermore, a simple relation was derived between the peak magnitude of the substrate stress and the interface stress, which was independent of the shape of the substrate stress profiles obtained. Interface strength strongly correlated with the PBO formulation and the surface roughness of the Si_xN_y layer. The interface strength was enhanced by including the dehydration bake procedure in the thin film processing steps. A significant amount of degradation in interface strength after autoclaving was observed for samples fabricated without the dehydration bake procedure.

Acknowledgements

This research was supported by Texas Instruments and National Science Foundation Grant CMS 04-08487.

Appendix

The analytical solution of wave propagation across a layer of finite length, h, sandwiched between two semi-infinite media is presented. The problem is visualized using the method of characteristics via the $(x-t)$ diagram shown in Fig. A.1. The two solid grey lines represent the boundary of the middle layer made of Material 2 (Si_xN_y). Material 1 (Si) and Material 3 (PBO) on either side of the center layer are assumed semi-infinite. The boundary, which separates Materials 1 and 2, is denoted by Interface I and the boundary between Materials 2 and 3 is denoted by Interface II. When a propagating stress pulse strikes the interface between two media of different material properties, part of the pulse is reflected and the remaining part is transmitted across the interface. By imposing continuity of tractions and displacements across the interface, the coefficients of transmission and reflection are derived in terms of the impedance mismatch ratio of the two materials. The equations governing the evolution of stress at Interfaces I and II as a function of time t under the influence of the substrate stress denoted by $\sigma^0_{i,\mathrm{I}}$, are given by Eq. (A.1) and (A.2), respectively:

$$\sigma_1(t) = A\sigma^0_{i,\mathrm{I}} + DCA\sum_{j=1}^{n}(EC)^{j-1}\sigma^0_{i,0}\left(t-\frac{2h}{C_{\mathrm{d},2}}j\right), \tag{A.1}$$

$$\sigma_{\mathrm{II}}\left(t-\frac{h}{C_{\mathrm{d}}}\right) = BA\sigma^0_{i,\mathrm{I}} + BA\sum_{j=1}^{n}(EC)^{j-1}\sigma^0_{i,0}\left(t-\frac{2h}{C_{\mathrm{d},2}}j\right), \tag{A.2}$$

where the coefficients of reflection and transmission at the interfaces, A–E, are given by

$$A=\frac{2\alpha_{\mathrm{I}}}{1+\alpha_{\mathrm{I}}}; B=\frac{2\alpha_{\mathrm{II}}}{1+\alpha_{\mathrm{II}}}; C=B-1; D=A/\alpha_{\mathrm{I}}; E=1-A.$$

The parameters α_{I} and α_{II} are the impedance mismatch ratios, which depend on the density (ϱ) and dilatational wave speed (C_{d}) through.

$$\alpha_{\mathrm{I}}=\frac{\partial_2 C_{\mathrm{d},2}}{\partial_1 C_{\mathrm{d},1}}; \alpha_{\mathrm{II}}=\frac{\partial_3 C_{\mathrm{d},3}}{\partial_2 C_{\mathrm{d},3}}.$$

The numbers in the subscript entering the above equation denote the interface number for α and material numbers for ϱ

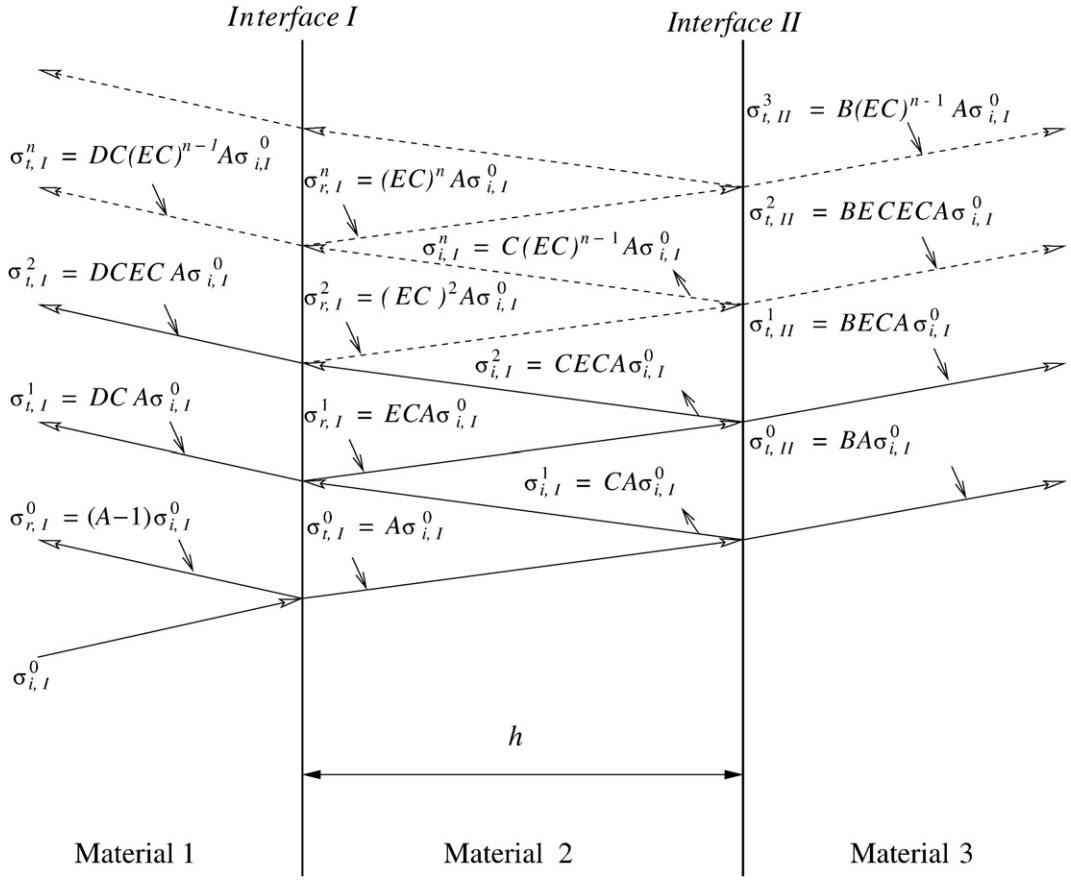

Fig. A.1. Schematic of the $x-t$ (space–time) illustrating the process performed to track the interface stress evolution using the method of characteristics. $\sigma^{c}_{a,b}$ denotes the stress associated with the reflected ($a=r$), incident ($a=i$) or transmitted ($a=t$) pulse at interface b (=I or II) for reflection c (=0, 1, 2, ...).

and C_d. The summation is carried over for each reflection j, beginning from 1 and ending with n (the total number of reflections).

In the case of a bi-material system, the solution reduces to

$$\sigma_{\mathrm{I}}(t) = A\sigma^{0}_{i,\mathrm{I}} - DA\sum_{j=1}^{n}(-E)^{j-1}\sigma^{0}_{i,0}\left(t - \frac{2h}{C_{\mathrm{d},2}}j\right). \qquad (A.3)$$

References

[1] R.H. Lacombe, Adhesion Measurement Methods: Theory and Practice, Boca Raton FL, CRC Press, 2006.
[2] D.Y. Shih, J. Kim, P. Buchwalter, P. Lauro, H. Clearfield, K.W. Lee, J. Paraszczak, S. Purushothaman, A. Viehbeck, S. Kamath, C. Lund, H.M. Tong, M. Anschel, R. Lacombe, 45th Electronic Components and Technology Conference, May 21–24, 1995, IEEE, Las Vegas, U.S.A., p. 884.
[3] J.J. Vlassak, Y. Lin, T.Y. Tsui, Mater. Sci. Eng. A 391 (2005) 159.
[4] T.Y. Tsui, A.J. McKerrow, J.J. Vlassak, J. Mech. Phys. Solids 54 (2006) 887.
[5] J. Hinkley, J. Adhesion 16 (1983) 115.
[6] A. Bagchi, G.E. Lucas, Z. Suo, A.G. Evans, J. Mater. Res 9 (1994) 1734.
[7] M. Modi, S.K. Sitaraman, J. Electron. Packag 126 (2004) 301.
[8] J. Zheng, S.K. Sitaraman, Thin Solid Films 515 (2007) 4709.
[9] J. Wang, R.L. Weaver, N.R. Sottos, J. Mech. Phys. Solids 52 (2004) 999.
[10] J. Wang, R.L. Weaver, N.R. Sottos, Exp. Mech. 42 (2002) 74.
[11] J. Wang, R. Weaver, N.R. Sottos, J. Appl. Phys 93 (2003) 9529.
[12] V. Gupta, R. Hernandez, J. Wu, P. Charconnet, Vacuum 59 (2000) 292.
[13] V. Gupta, A.S. Argon, J.A. Cornie, D.M. Parks, Mater. Sci. Eng. A 126 (1990) 105.
[14] V. Gupta, A.S. Argon, J.A. Cornie, D.M. Parks, J. Mech. Phys. Solids 40 (1992) 141.
[15] V. Gupta, J. Yuan, A. Pronin, J. Adhes. Sci. Technol 8 (1994) 713.
[16] J. Yuan, V. Gupta, Acta Metall. Mater 43 (1995) 781.
[17] J. Yuan, V. Gupta, J. Appl. Phys 74 (1993) 2388.
[18] J. Yuan, V. Gupta, J. Appl. Phys 74 (1993) 2397.
[19] J. Yuan, V. Gupta, J. Appl. Phys 74 (1993) 2405.
[20] M. Boustie, E. Auroux, J.P. Romain, A. Bertoli, D. Manesse, Eur. Phys. J. — Appl. Phys. 5 (1999) 149.
[21] C. Bolis, L. Berthe, M. Boustie, M. Arrigoni, S. Barradas, M. Jeandin, J. Phys. D Appl. Phys. 40 (2007) 3155.
[22] R. Dias, IEEE T. Device Mater. Reliab. 3 (2003) 179.
[23] J.L. Vossen, in: K.L. Mittal (Ed.), Adhesion Measurement of Thin Films, Thick Films, and Bulk Coatings, American Society for Testing and Materials, STP, vol. 640, 1978, p. 122.
[24] A. Jain, V. Gupta, S.N. Basu, Acta Mater. 53 (2005) 3147.
[25] L.M. Barker, Exp. Mech. 12 (1972) 209.
[26] M. Miller, M. Mello, 52nd Electronic Components and Technology Conference, May 28–31, 2002, p. 192, San Diego, U.S.A.
[27] F.Z. Ren, P. Liu, S.G. Jia, B.H. Tian, J.H. Su, Mater. Sci. Eng. A 419 (2006) 233.